AD_____
(Leave blank)

Award Number:
W81XWH-08-1-0189

TITLE:
Optimization of the Temporal Pattern of Applied Radiation Dose: Implication for the Treatment of Prostate Cancer

PRINCIPAL INVESTIGATOR:
Michael Altman

CONTRACTING ORGANIZATION:
University of Chicago
Chicago, IL 60637

REPORT DATE:
March 2009

TYPE OF REPORT:
Annual Summary

PREPARED FOR: U.S. Army Medical Research and Materiel Command
Fort Detrick, Maryland 21702-5012

DISTRIBUTION STATEMENT: (Check one)

X Approved for public release; distribution unlimited

Distribution limited to U.S. Government agencies only; report contains proprietary information

REPORT DOCUMENTATION PAGE

Form Approved
OMB No. 0704-0188

1. REPORT DATE *(DD-MM-YYYY)*	2. REPORT TYPE	3. DATES COVERED: *1 MAR 2008-28 FEB 2009*
31-03-2009	Annual Summary	

4. TITLE AND SUBTITLE
Optimization of the Temporal Pattern of Applied Radiation Dose: Implication for the Treatment of Prostate Cancer

5a. CONTRACT NUMBER

5b. GRANT NUMBER
W81XWH-08-1-0189

5c. PROGRAM ELEMENT NUMBER

6. AUTHOR(S)
Michael Altman

5d. PROJECT NUMBER

5e. TASK NUMBER

5f. WORK UNIT NUMBER

7. PERFORMING ORGANIZATION NAME(S) AND ADDRESS(ES)

University of Chicago
970 East 58th Street
Chicago IL, 60637

8. PERFORMING ORGANIZATION REPORT NUMBER

9. SPONSORING / MONITORING AGENCY NAME(S) AND ADDRESS(ES)
U.S. Army Medical Research and Materiel Command
Fort Detrick, Maryland 21702-5012

10. SPONSOR/MONITOR'S ACRONYM(S)

11. SPONSOR/MONITOR'S REPORT NUMBER(S)

12. DISTRIBUTION / AVAILABILITY STATEMENT
Approved for public release; distribution unlimited

13. SUPPLEMENTARY NOTES

14. ABSTRACT
Our previous modeling study demonstrated that the temporal pattern of applied dose during a single fraction of radiation can impact cell survival, especially in situations with low α/β and large dose/fx and fraction length (T_f). Two different arrangements of the same set of radiation fields were applied to low and high α/β cell lines at a high dose/fx and long T_f; a low α/β line was subjected to the same experiment at a low dose/fx, then a short T_f. Comparison of cell survival between both field arrangements agreed with the modeling study: statistically significant differences for the low α/β lines at high dose/fx and long T_f but not in any other case. To analyze temporal effects *in vitro* in a realistic treatment environment, a specialized phantom was characterized. Thermoluminescence dosimeters and film showed good agreement with dose predicted by a clinical treatment planning algorithm. A separate experiment showed good cellular response agreement with the phantom versus traditional experimental setups. These results show that the phantom is a useful tool to assess integration of temporal optimization into prostate cancer treatment planning, as these temporal optimization techniques could prove an important element in enhancing the efficacy of prostate cancer radiation therapy.

15. SUBJECT TERMS Prostate cancer; Radiation Therapy; Intensity Modulated Radiation Therapy; Radiobiology; *In vitro* experiments; Phantoms; Temporal Optimization, Linear-quadratic model, hypofractionation

16. SECURITY CLASSIFICATION OF:			17. LIMITATION OF ABSTRACT	18. NUMBER OF PAGES	19a. NAME OF RESPONSIBLE PERSON
a. REPORT	b. ABSTRACT	c. THIS PAGE			USAMRMC
U	U	U	UU	28	19b. TELEPHONE NUMBER *(include area code)*

Table of Contents

Page

INTRODUCTION

External beam radiation therapy (EBRT) is a frequently used tool in the treatment and management of prostate cancer. One of the standard treatments for prostate cancer has been three dimensional conformal radiation therapy (3DCRT) , in which the radiation fields are conformed to the shape of the prostate at each angle, allowing for irradiation of the prostate while limiting the irradiated volume of the surrounding normal tissues [1, 2]. Recently, intensity modulated radiation therapy (IMRT) has become an increasingly popular form of radiation therapy for many forms of cancer, including prostate cancer. IMRT, a more complex radiation delivery scheme than 3DCRT, uses beams which are modulated throughout treatment to produce radiation fields of non-uniform intensity [3-5]. These non-uniform fields provide three dimensional dose distributions which more closely conform to the shape and volume of the prostate than 3DCRT; with greater conformity comes a larger reduction of dose to the surrounding normal tissues, limiting radiation induced complications of treatment and organ failure [6-10].

The greater complexity of IMRT results in longer treatment times for a single treatment session or fraction of radiation. The rising prevalence of IMRT as a treatment modality has given rise to a number of studies investigating the impact of temporal effects in IMRT, especially as they relate to the radiobiology of the underlying tissue [11-17]. There is thus an increasing recognition of the interaction between increasing single fraction radiation therapy treatment times and cell repair. The capacity for cell repair directly effects cell survival, thus the understanding of these temporal effects may have clinically relevant implications with regard to tumor control and normal tissue sparing [18-24].

The temporal effects relating to radiation therapy (RT) are generally analyzed in terms of cell survival using the linear quadratic (LQ) model [25-28]. For a single IMRT fraction, the LQ model is given by

$$S = \exp-(\alpha D + \beta G(t) D^2) \qquad (1)$$

where D is the dose per fraction (dose/fx), α and β relate to the tissue's ability to repair radiation damage, and G(t) is the Lea-Catcheside dose protraction factor, also known simply as the dose protraction factor. G(t) accounts for the time variables involved in RT. In its most general form, G(t) is given, at a time t, by [29]:

$$G(t) = \frac{2}{D^2} \int_0^t dw\, I(w) \int_0^w dv\, I(v)\, e^{-\mu(w-v)} \qquad (2)$$

where D is the dose per fraction (dose/fx), I(k) is the dose rate at time k, $\mu = \ln 2 / T_{1/2}$, where $T_{1/2}$ is a tissue specific repair half-time, and w and v are time variables. The LQ model is dependent on two time-related factors which correlate to radiobiological effects. The first of these is the "fraction duration," the total time measured beginning when the first radiation beam is "turned on" and ending when the last beam is "turned off." The limits of integration of the outer integral in Eq. 2 can be viewed as the beginning and end of the time span defined by the fraction duration (T_f). The effect of fraction duration on cell kill has been well studied, with an increasing fraction

duration yielding a larger surviving fraction [11, 13, 16, 17, 19-24]. The other time variable which may affect the degree of cell kill is the functional form of *how* the dose is applied over time, or "temporal pattern of applied dose." This is due, in Eq. 2, to the double integration. There has been some previous implication that the temporal pattern of applied dose during treatment may impact the degree of cell kill [18, 27, 30-33]. However, we performed the first in-depth investigation of the effect of the temporal pattern of applied dose, especially with regards to IMRT [34].

This model-based study revealed techniques for temporal manipulation of the dose arrangement to maximize or minimize cell kill. Cell kill was found to be maximized using a "Triangle" dose pattern in which the highest dose fields of a plan are clustered in the middle of a treatment fraction and the lowest doses distributed between the beginning and end. A "V-shaped" pattern, in which the lowest dose fields were clustered at the center of a treatment fraction and the highest dose fields are distributed between the beginning and end of a treatment fraction, was found to minimize cell kill. The study also investigated the impact of three variables associated with a single fraction of IMRT that can interact with variations in the temporal pattern of applied dose to affect cell kill: irradiated tissue type (in terms of α/β), fraction duration, and dose per fraction (dose/fx). The modeling study found that the effects of the temporal pattern of applied dose are greatest in treatments which irradiate tissues with lower α/β, use longer fraction durations and/or large doses/fx.

The "optimized" dose patterns described by the modeling study could potentially influence prostate cancer treatment outcome. This is because integration of temporal optimization a treatment planning algortithm could be used to enhance tumor cell kill, improving prostate tumor control, or decrease cell kill in normal tissues such as bladder and rectum to reduce radiation sequeulae. However, before conclusions of the modeling study can be integrated into clinical techniques, they must first be validated *in vitro*. Then steps need to be taken to integrate temporal optimization into a treatment environment and test the ability to delivery such a treatment. This begins with the development of a phantom for use in three dimensional radiobiology experiments in a realistic treatment environment. Then a scheme to implement temporal optimization into an IMRT-based prostate cancer treatment plan needs to be developed and analyzed.

Our hypothesis is that the temporal pattern of applied dose in a single fraction of radiation can be optimized to maximize or minimize cell kill. Furthermore, irradiation with a treatment plan incorporating such techniques will provide differential cell kill across various structures of interest, such as prostate tumor, bladder, and rectal tissues, compared with irradiation using a treatment plan derived from standard-based methods.

BODY

There are three main tasks associated with this project. Within each there are one or more subtasks, each of with has several objectives. Progress made on the following tasks programmed to be addressed in the first year of the project is as described below:

Task I: Validate the modeling study *in vitro*

A manuscript based on the data and conclusions resulting from accomplishment of the objectives and subtasks of Task I has been submitted for publication, although not as of yet accepted. The discussion of the accomplishment of these subtasks and objectives below contains excerpts from this submission.

I.A: Experimentally determine radiobiological parameters of cell lines of interest in vitro. (1-5 mos.)

Objectives:

1. Determine cell lines of interest. (1-2 mos.)
2. Perform *in vitro* experiments on all cell lines of interest to measure parameters, repeating experiments to ensure result consistency as needed.(2-4 mos.)
3. Analyze survival data to determine radiobiological parameters. (4-5 mos.)

As noted above, the modeling study predicted that temporal optimization effects were greatest for tissues with low α/β. For a comparative analysis, the "cell lines of interest" as defined in Subtask I.A Objective 1 should include at least one low α/β line and one high α/β line. It should also be noted that the modeling study held α constant, meaning there was also an implicit dependence on β. As the temporal factors couple to the β term in the LQ model (Eq. 1), the impact of the temporal pattern of dose will be stronger in cases with higher β. However, in terms of overall cell survival, a cell line more susceptible to repairable relative to irreparable damage (thus low α/β) is also important. Ultimately, this means that the greatest opportunity to see differences is if the low α/β cell lines of interest for this study also have high β, while the high α/β cell lines used have low β. As we plan to measure cell survival following radiation using the clonogenic cell survival assay, we also require that the cell lines we use be clonogenically useful. That is, they should form good, countable colonies for clonogenic evaluation.

Following investigation of the on-site departmental tissue culture bank, we found three candidates which satisfied our requirements: WiDr, a colonic adenocarcinoma line, PC-3, a prostate carcinoma line, and SQ-20B, a head-and-neck squamous cell carcinoma line. Previously acquired clonogenic survival data for these cell lines implied that that PC-3 and WiDr were lower α/β and higher β cell lines, while SQ-20B had a higher α/β and lower β.

Subtask I.A Objectives 2-3 involved the experimental measurement of the radiobiological parameters of each cell line used in the completion of Task I. Measurement of α and β from Eq. 1 intertwines with the previous objective, in that the measurement of these parameters verifies that they indeed satisfy the requirements outlined above. α and β were measured by creating survival curves for each cell line using the clonogenic survival assay. The survival curves were created by irradiating cells over a range of doses from 0-10 Gy and determining the percentage of cells surviving at each of the dose points analyzed. Acute irradiations were used, eliminating the impact of the dose protraction factor in Eq. 1 (i.e. as the dose rate , I in Eq. 2, gets very large, $G(t) \rightarrow 1$). Eq. 1, with $G(t)=1$, is then fit to the resultant percent survival versus acute dose curves to determine α and β.

Cells were maintained in appropriate media at 37° C and 7% CO_2. Taking into consideration the cell line and experimental treatment, cells were plated in 6-well plates at densities predetermined to yield 60-100 surviving colonies per well. A non-irradiated control with 100 cells/well was also plated for each cell line and experiment performed. Prior to irradiation, cells were incubated for 12-24 h in a final volume of 2 ml/well.

Cells were then irradiated with each cell line being irradiated individually. After radiation application, cells were incubated at 37°C and 7% CO_2 for 10 days, at which time a clonogenic survival assay was performed. Plates were washed with 1X phosphate buffer solution, and then stained with 2% crystal violet in 50% ethanol for one hour. Excess stain was washed off and surviving colonies (containing ≥50 cells) were counted by eye. The treatment (Triangle or V-shaped) of the plates was blinded to the observer. A single observer counted all events and comparisons were done across four independent observers to validate the results. The average number of events per plate exceeded 400. Surviving fraction was calculated for each well after factoring in the plating efficiency (PE) determined from the control plates. Each experiment (i.e. a specific cell line, fraction duration and total dose combination) was performed multiple times.

Average parameters measured using these techniques validated these original assertions regarding each cell line, with WiDr having α/β=3.39 Gy (β=0.046 Gy^{-2}), PC-3 having α/β=5.56 Gy (β=0.046 Gy^{-2}), and SQ-20B having α/β=8.72 Gy (β=0.016 Gy^{-2}). As "lower α/β" cell lines (WiDr and PC-3) also had higher β values than SQ-20B, we will use the low vs. high α/β or high vs. low β designations interchangeably in this report.

The measurement of the radiobiological parameters related to the G(t) function proved far more difficult. Initially, this might not seem the case, with only one tissue specific parameter, μ, in Eq. 2. While μ is typically defined as $\ln(2)/T_{1/2}$, Fowler *et al.* [11] notes that $T_{1/2}$ continuously changes with time and that two $T_{1/2}$ values, with properly weighted corresponding G(t) functions, is a reasonable approximation. This is the approach taken in the previously discussed modeling study. Thus to get an accurate model, at least four additional parameters (two $T_{1/2}$s and two weights) would need to be measured for each cell line. A series of "split dose" experiments, in which cells were irradiated with two equal acute doses split by a time, T, were performed on each cell line. In this specialized case, G(t) reduces to:

$$G(t) = \frac{w_1}{2}\left(1 + e^{-\mu_1 T}\right) + \frac{w_2}{2}\left(1 + e^{-\mu_2 T}\right) \qquad (3)$$

where w_x are the weights and μ_x are the corresponding μ values. Fig. 1 shows an example PC-3 split dose experiments over a range of T values from 0-40 min. Recall that the surviving fraction can be related to G(t) from Eq. 1. Using the measured α and β values for a given cell line, we attempted to fit Eq. 3 to the data measured for each cell line, but given the errors in each data point, we found the parameter fitting would either give unrealistic results or confidence intervals so wide that virtually any measured data would fit the model. One option to resolve this would perhaps be to acquire date with a finer split time sampling than we have done. However, the inherent errors of the clonogenic assay means that much finer time sampling would not give useful results: for example, in Fig.1, calculations with the Mann-Whitney U test show the differences in surviving fraction between all points ≥10 minutes split time do not show statistical

significance ($p > 0.05$). Other methods we used to attempt to estimate G(t) from experimental data for more complex temporal dose patterns suffered similarly from the inability to differentiate temporal data points using the clonogenic assay.

We were thus unable to directly measure all the radiobiological parameters to determine if the temporal optimization effects analyzed below in Subtask II.B matched the radiobiological models of Eqs. 1-2. Our alternative solution was to analyze the entire parameter space of the modeling study to validate its conclusions. In other words, will we strive, as originally programmed, to show that there is a statistically significant difference in cell survival between irradiation with a Triangle versus V-shaped dose pattern for low α/β cell lines at high dose/fx and long T_f. Then, however, we will analyze the comparative effects of temporal optimization using a higher α/β cell line, low dose/fx, or short T_f.

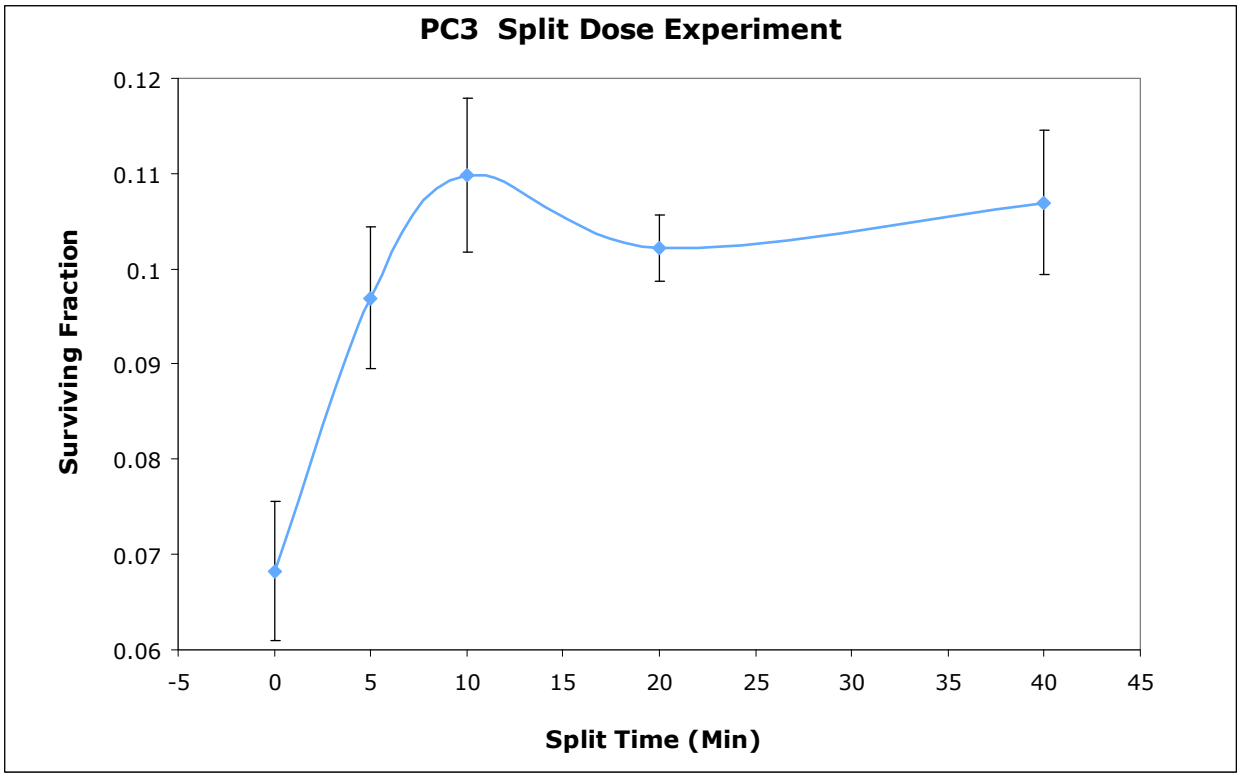

Figure 1: Results from an example split dose experiment on PC-3 cells. Error bars represent the standard error at each analyzed split time. Total dose was 6 Gy for all points.

I.B: In vitro experimental verification of previous modeling study. (3-6 mos.)

Objectives:

1. Perform *in vitro* experiments on cell lines of interest, repeating experiments to ensure result consistency as needed. (3-5 mos)
2. Analyze of survival data and assess results in comparison to assertions of the modeling study. (5-6 mos.)

WiDr, PC-3, and SQ-20B cells were all irradiated and survival evaluated in Subtask I.B using the clonogenic assay as described above in Subtask I.A. As the dose patterns in Subtask I.B are designed to emulate clinically used IMRT irradiation schemes, irradiation was performed using a clinical linear accelerator (2100CD, Varian Medical Systems, Palo Alto, CA) delivering 6 MV photons at 600 MU/min. Each six-well plate was irradiated individually. The plate was placed in a phantom composed of a rectangular block of solid water with a plate-sized cavity (8.6 x 12.8 x 2.0 cm) at the center. Radiation was delivered with a 20 x 20 cm field at 90 cm SSD and 10 cm depth (i.e. to the bottom of the plate, where the cells were). Dosimetry in the phantom was assessed with film and monitor units were calculated accordingly to deliver the desired dose.

Once in the phantom, each plate was irradiated with 900 cGy divided into six fields, delivered over 20 minutes (T_f =20 min). The six fields were comprised of two fields each of 325 cGy, 100 cGy, and 25 cGy with the temporal midpoints (times at which half the dose of an individual field has been delivered) equally distributed over T_f. Two plates of each cell line were irradiated, one with the fields arranged in a Triangle pattern, and another with the fields arranged in a V-shaped pattern (Fig. 2). During this, as well as any other Triangle/V-shaped irradiation pair, only the order in which the radiation fields are delivered changes. Following irradiation, cells were incubated for 10-14 days, stained, and counted as described above in Subtask I.A. Surviving fraction was also calculated as described above.

Analysis of the parameter space of the modeling study was achieved through three separate but complementary experiments. The high α/β SQ-20 cells were included in the experiments just described to determine the effects of changing tissue type. Then, separate plates of WiDr cells, the lowest α/β and highest β line, were subjected to two additional radiation patterns. In one of these, two WiDr plates were irradiated with the same patterns and T_f as in Fig. 1 with each of the six fields reduced by 80%, resulting in a total dose of 180 cGy; by comparing this to the 900 cGy results, the effect of dose/fx was analyzed. Then two plates were irradiated with the same patterns and doses/field as in Fig. 1, but with T_f =5 min, measuring the effect of changing T_f.

The analysis described in Subtask I.B Objective 2 was done statistically on each individual experiment. For each set of irradiation conditions (cell line, T_f, dose/fx), the surviving fractions of cells from each well in the plate irradiated with the triangle irradiation pattern was compared to the measured surviving fractions from the corresponding V-shaped pattern irradiated plate through p-values calculated with the one-tailed Mann-Whitney U-test [35]. Statistically significant differences were assumed at the $p<0.05$ level.

An average normalized surviving fraction for irradiation with the Triangle (S_{Tri}) and V-shaped (S_V) patterns was calculated for each individual experiment by averaging the measured normalized surviving fraction from all six wells in the corresponding plates for that experiment. The standard error in each S_{Tri} and S_V was calculated, using standard error propagation techniques, from the standard deviation of the PE value for that experiment and the standard deviation of the corresponding non-normalized surviving fractions used to calculate each factor.

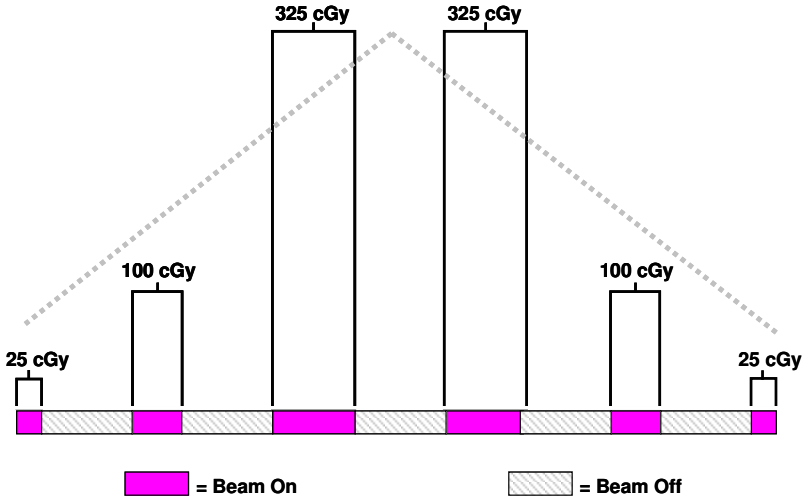

(a)

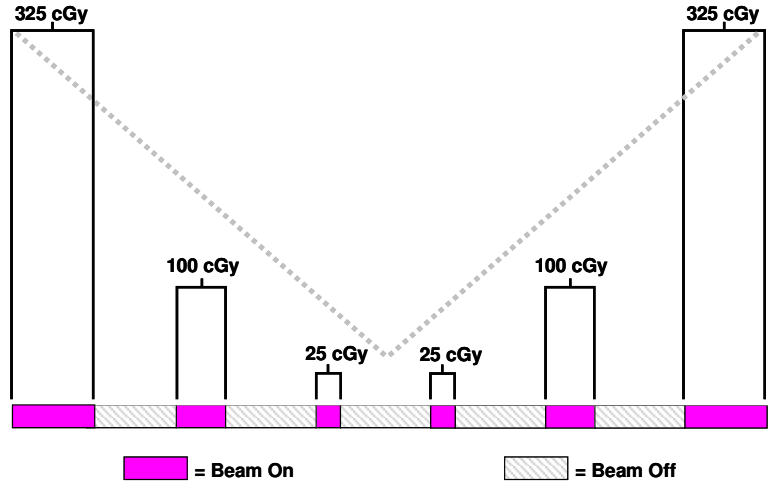

(b)

Figure 2: a) A schematic of the six field 900 cGy dose pattern used to irradiate cells. Here the fields have been arranged in the "Triangle" pattern (dashed line) which yields maximum cell kill. In the figure, the horizontal axis represents time. b) The same as (a), except a representation of the "V-shaped" dose pattern (dashed line) to yield minimum cell kill. Note the exact same fields are used in both (a) and (b) and the duration of delivery is exactly the same – only the order in which they were delivered has been changed.

All three cell lines analyzed were irradiated with the dose patterns in Fig. 2 to a total dose of 900 cGy over 20 min. Figs. 3a-c show the measured S_{Tri} and S_V values for PC-3, WiDr, and SQ-20B, respectively, for all three experimental iterations on each cell line. Above each S_{Tri}/S_V pair is the corresponding p-value for that experiment. Note that for the high-β cell lines, WiDr (Fig. 3a) and PC-3 (Fig. 3b), there is a consistent, visible increase in surviving fraction when irradiating with the V-shaped pattern versus the Triangle pattern. Furthermore, $p<0.05$ for each individual WiDr and PC-3 experiment, indicating that the increase in survival from Triangle to V-shaped irradiation is statistically significant in all cases. These results show that tangible differences in cell survival can be achieved simply by rearranging the temporal pattern of applied dose.

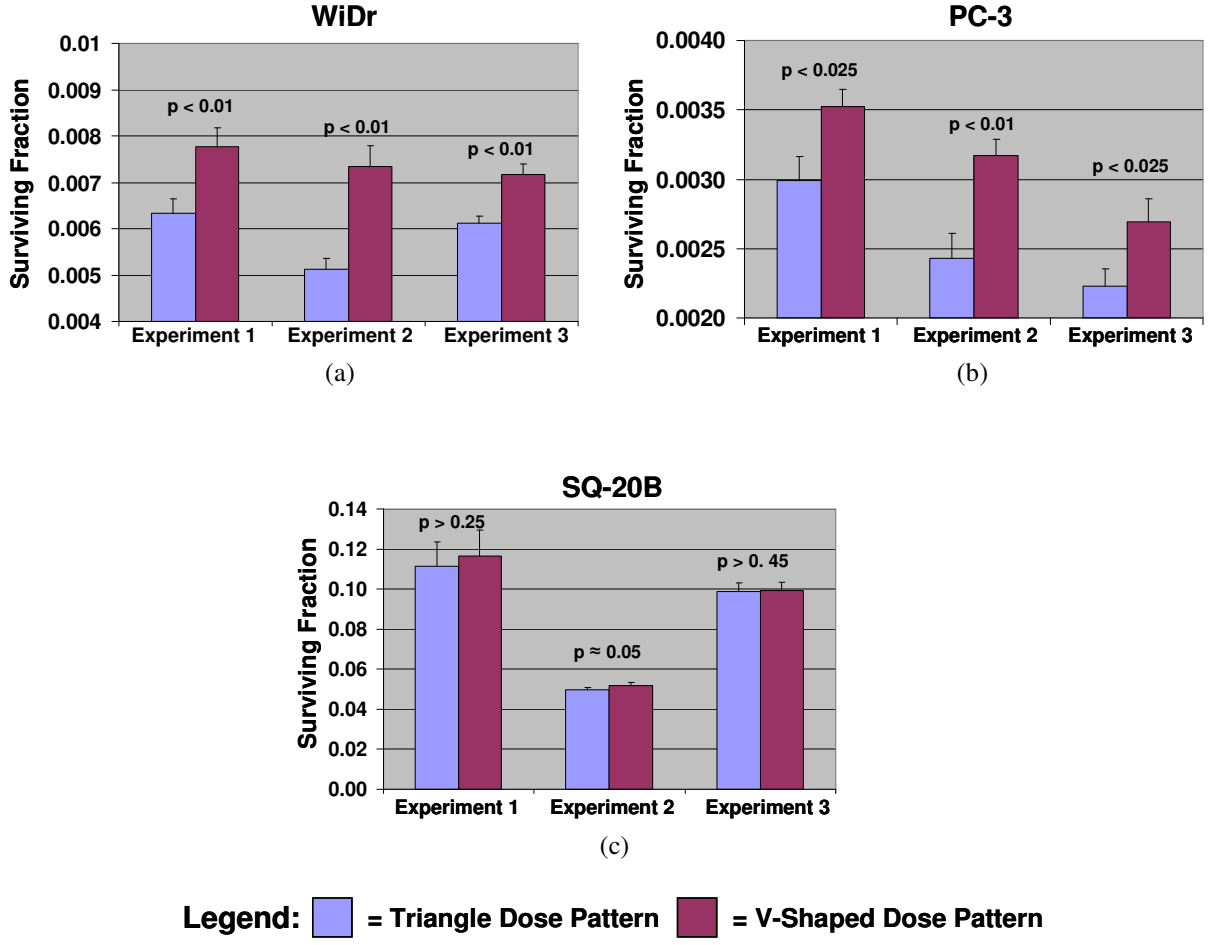

Figure 3: Comparison of surviving fraction of cells following irradiation with the Triangle dose pattern versus the V-shaped dose patterns as discussed in the text using a total dose 900 cGy and fraction duration of 20 min. a) WiDr cells, b) PC-3 cells, and c) SQ-20B cells. For each combination of cell line and irradiation condition, three independent experimental iterations were performed (marked Experiments 1-3 on graphs). One tailed p-values calculated using the Mann-Whitney U-test for all experimental iterations in all cell line-irradiation condition combinations are shown above

The high-α/β SQ-20B cells show a radically different picture. In Fig. 3c the visible differences seen for the WiDr and PC-3 cells are minimal or nonexistent. The comparative statistics for each SQ-20B experiment either did not show statistically significant differences between the populations ($p>0.05$ for iterations 1 and 3) or borderline statistically significant differences ($p\approx0.05$ for iteration 2). This loss of persistent, statistically significant differences for the same irradiation patterns and parameters applied to the SQ-20B cells agrees with the assertion of the modeling study that differences in cell survival between irradiation with the Triangle and V-shaped patterns decrease with increasing α/β [34].

Figs. 4a,b show the same comparisons for the WiDr cells when irradiated with 180 cGy over 20 min, or 900 cGy over 5 min, respectively. The consistent increase in survival when irradiating with the V-shaped dose pattern compared to the Triangle dose pattern as seen for the 900 cGy/20 min irradiation in Fig. 3a is absent. Furthermore for all experimental iterations of both the 180 cGy/20 min and 900 cGy/5 min irradiations the populations receiving Triangle and V-shaped dose patterns do not show statistically significant differences ($p>0.05$). These results both agree with the modeling study, which predicted that the increase in cell survival between irradiation with the Triangle versus V-shaped dose patterns is larger with greater dose/fx and/or T_f [34].

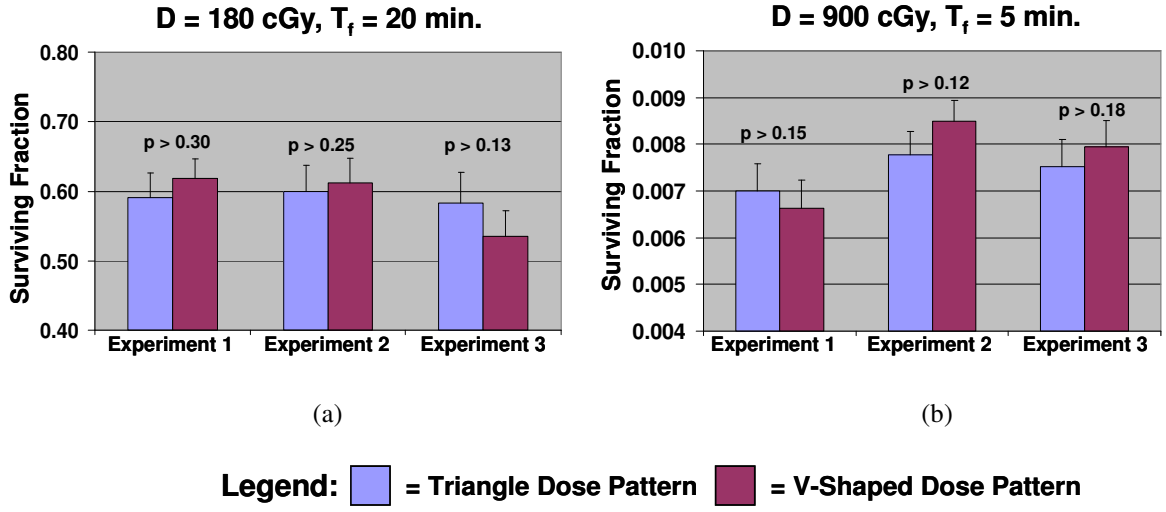

Figure 4: Similar comparison to Fig. 3a of surviving fraction of WiDr cells following irradiation with the Triangle dose pattern versus the V-shaped dose patterns as discussed in the text for a) a total dose (D) of 180 cGy and fraction duration (T_f) of 20 min b) D =900 cGy and T_f =5 min. Unlike Fig. 3a, p-values above each corresponding Triangle/V-shaped survival pair do not show statistically significant differences.

We then completed Subtask I.B Objective 2 by calculating the average difference in surviving fraction when irradiating with the Triangle versus V-shaped dose pattern for each set of irradiation conditions. These were then compared to corresponding values predicted by the modeling study. The average measured percent change in survival between irradiation with the Triangle and V-shaped pattern ($\Delta\%S_{Tri\text{-}V}$) was calculated for each set of irradiation conditions by:

$$\Delta\%S_{Tri-V} = \tfrac{1}{3}\sum_{n=1}^{3}\frac{S_{V,n} - S_{Tri,n}}{S_{V,n}} \cdot 100 \qquad (4)$$

where n = 1,2,3 represent the three experimental iterations performed for each set of conditions. Standard errors in $\Delta\%S_{Tri\text{-}V}$ were again calculated using standard propagation methods.

This data was compared to that predicted by the theoretical models by substituting Eq. 1 into Eq. 3 (ignoring the summation):

$$\Delta\%S_{Tri-V} = \left[1 - \exp\left(\beta\left(G_{Tri}(t) - G_{V}(t)\right)D^{2}\right)\right] \cdot 100 \qquad (5)$$

where $G_{Tri}(t)$ and $G_V(t)$ were calculated using the corresponding temporal patterns, Eq. 2, and the techniques (including population-average tissue-dependent parameters) of the modeling study [34]. We used the population average parameters to calculate the G(t) values for reasons previously discussed in Subtask I.A. The β values were those we previously measured.

These relationships between the measured and calculated $\Delta\%S_{Tri\text{-}V}$ values can be seen in Fig. 5. $\Delta\%S_{Tri\text{-}V}$ was 21.2+/-2.5% for the WiDr cells and 18.6+/-4.7% for the PC-3 cells at 900 cGy/fx and T_f=20 min. For the higher α/β SQ-20B cells this drops to $\Delta\%S_{Tri\text{-}V}$=3.0+/-1.3%. Irradiating WiDr cells with 180 cGy/fx over 20 min resulted in $\Delta\%S_{Tri\text{-}V}$=2.7+/-4.1%, while irradiating them with 900 cGy/fx over 5 min yielded $\Delta\%S_{Tri\text{-}V}$=-0.8+/-4.2%. Fig. 5 shows that these results compare very favorably to those predicted by the model, although the model-predicted values should only be seen as rough estimates due to the errors in the measured β values and the use of population average parameters in the calculation of $G_{Tri}(t)$-$G_V(t)$ (Eq. 4). Ultimately, measurement and theory display the same patterns throughout: relatively large increase when comparing the surviving fraction of cells irradiated with the Triangle dose pattern versus the V-shaped for low-α/β cell lines, large doses/fx and long T_f. However, if α/β is decreased, the dose/fx is decreased, or T_f is shortened, these differences diminish.

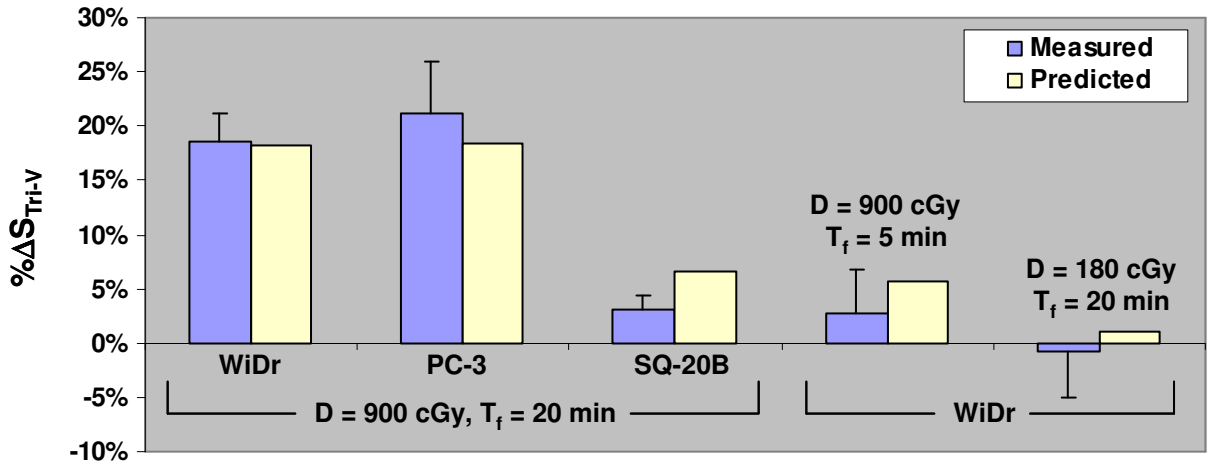

Figure 5: Average percent change in surviving fraction (%ΔS) between irradiation with the Triangle and V-Shaped dose pattern for each cell line and irradiation condition combination shown in Figs. 4 and 5 (blue bar). Error bars on these curves indicate the standard error in the %ΔS amongst the three experimental iterations performed for each set of conditions. Yellow bars indicate the %ΔS values predicted using the measured α/β values for each cell line (see text) along with other average population parameters [34].

Task II: Characterize a phantom for use in three-dimensional *in vitro* experiments in a realistic treatment environment

II.A: Characterization of dosimetry in IMRT radiobiological experiment phantom using TLDs and film. (7-10 mos.)

Objectives:

1. Create IMRT treatment plan(s) for phantom. (7-8 mos.)
2. Determine consistently responding TLD set for experiment. (7-8 mos.)
3. Characterize phantom dosimetry with TLDs and film. (8-10 mos.)
4. Analysis of measured dosimetry with TLDs and film compared to predicted dosimetry from treatment planning software. Determine a scheme for reconciliation of the two as needed. (9-10 mos.)

All of the objectives of subtask II.A were completed. The data and analysis were published as Altman *et al.* "Characterization of a novel phantom for three-dimensional *in vitro* cell experiments." *Phys Med Biol.* 2009; 54(5):N75-N82. This paper has been attached in the appendix of this report; it will provide an in depth summary and analysis of the completion of the objectives in subtask II.A.

II.B: Assess the effectiveness of the phantom as a tool for performing in vitro experiments. (10-14 mos.)

Objectives:

1 Experimental design and setup (10-11 mos.)
2. Perform *in vitro* experiments, repeating experiments to ensure result consistency as needed. (11-13 mos.)
3. Analyze results to determine if equivalency with standard in vitro experimental techniques is feasible (13-14 mos.)

The effectiveness of the phantom as a tool for performing in vitro experiments was assessed through a biological validation using two human cancer A549 [36, 37], a lung adenocarcinoma (obtained from the American Type Culture Collection), and SCC116 [38], an alveolar ridge squamous cell carcinoma (acquired from the lab of Dr. Susanne Gollin at the University of Pittsburgh). Cells were analyzed using the diphenylamine (DPA) assay, which measures DNA accumulation or loss, and can be used to calculate the percent of viable cells post-irradiation (%Via) [39]. In contrast to the clonogenic survival assay, the colorimetric nature of the DPA assay means that more data points can be efficiently collected. Furthermore, the automated readout systems used to analyze DPA assays limit the human error often associated with counting colonies in the clonogenic assay. All chemicals used in the preparation of solutions needed for the assay were purchased from the Sigma-Aldrich Chemical Company and used as received. Cells were seeded (100 μL) into 96-well plates and grown until they were approximately 50-60% confluent. Nine identical plates were prepared, with one (randomly selected) of these serving as the unirradiated control. Three hours prior to irradiation, an additional 150 μL of media was added to each well.

The plates were irradiated using two different experimental setups: a "standard" setup similar to that used in a typical radiobiological experiment described earlier, and one employing the IMRT phantom. In both cases, doses of 1, 2, 5, and 10 Gy were delivered to the cell lines using the linear accelerator. In the standard setup, each dose was imparted using a single gantry angle (0°) to one 96-well plate placed within a solid water block. 6 MV photons were delivered at 600 MU/min with the well plate at the center of a 20 x 20 cm^2 field at 90 cm SSD and 10 cm depth. For the IMRT setup, a treatment plan was created which contained two ~235 cm^3 PTVs, each containing four rows of eight wells of all plates. Six equally-spaced beam angles were used, ranging from 28°-336°. Each PTV resided at opposite ends of the well plates. The ratio of doses between the two PTVs was fixed at 2:1. Two plans were created to deliver nominal doses of 1 and 2 Gy, and 5 and 10 Gy to the proximal and distal PTVs, respectively. The phantom was loaded with two well plates per plan.

Immediately following irradiation, the plates were placed back in the incubator for an additional 96 hours. After this time, the media was completely removed from the cells, and 60 μL of a 1:5 mixture of chilled acetaldehyde (0.16% in water) and perchloric acid (20% vol/vol) was added. Each well was then treated with 100 μL of a 4% DPA solution in glacial acetic acid, and the plates were incubated for an additional 24 hours at 37 °C. The absorbance was then read at 595 nm for each well. Individual trials were normalized to mean readings from the unirradiated control plates to calculate the %Via values, which were then averaged.

For each cell line, single iterations of the biological validation experiment were analyzed separately. The error in every measured %Via was determined from the average σ^2 of all the points under the same irradiation conditions and that of the unirradiated control readings using standard error propagation techniques. The average %Via standard deviation for each irradiation

condition of the experiment was then calculated. For a given dose point, the %Vias generated using the two different experimental setups were compared using student t-tests.

For both the IMRT phantom and the standard setup, average %Vias and associated standard deviations from three independent experiments was calculated for both SCC116 and A549 cells at several dose points from 0-10 Gy (Table 1). The differences in %Via averaged 1.28% and 3.26% for the SCC116 and A549 cells, respectively. The results for the two experimental setups revealed $p>0.05$ when compared with the student t-test for both cell lines at all dose points. As the differences in %Via do not show statistical significance for either cell line, this implies that experimental results acquired in the phantom could be compared to or evaluated against results from previous or future studies employing more standard techniques.

Table 1: Percentage of viable cells post-irradiation measured using the DPA assay for two different cell lines.

Cell Line	Dose (cGy)	Percentage of Viable Cells Post-Irradiation (%)				
		Standard Setup		IMRT Phantom		Absolute Difference*
		Average	Standard Error	Average	Standard Error	
SCC116	100	89.23	8.04	87.40	8.91	1.84
	200	72.25	9.45	73.15	7.38	0.90
	500	31.15	5.51	30.38	3.71	0.76
	1000	12.30	3.28	13.94	4.20	1.63
A549	100	55.35	8.66	60.59	12.38	5.24
	200	34.49	7.74	38.22	8.15	3.73
	500	14.24	4.24	17.59	5.14	3.35
	1000	13.64	8.76	12.93	5.04	0.71

Abbreviations: DPA = diphenylamine IMRT = Intensity modulated radiation therapy

* Absolute difference is between the average percentage of viable cells post-irradiation from the standard setup and IMRT phantom. At each dose point, all differences show $p > 0.05$.

KEY RESEARCH ACCOMPLISHMENTS

- Determined cell lines of interest for *in vitro* experiments.
- Showed the effect of the rearrangement of the temporal pattern of applied dose for a single fraction of radiation *in vitro* is statistically significant for low α/β cell lines at high dose/fx and long fraction duration, as predicted by the previously published modeling study.

- Showed that temporal pattern based statistically significant differences disappear *in vitro* with increasing α/β, decreasing dose/fx, or decreasing fraction duration, results which also agree with conclusions of the modeling study.

- Verified dosimetrically that patient-based treatment plans can be accurately projected into a new phantom for use in three dimensional *in vitro* experiments.

- Performed a biological validation study showing that the use of the phantom is equivalent to established radiobiological experimental techniques.

REPORTABLE OUTCOMES

Original Peer-reviewed Publications:

Altman MB, Vesper BJ, Smith BD, Stinauer MA, Pelizzari CA, Aydogan B, Reft CS, Radosevich JA, Chmura SJ, Roeske JC. Characterization of a novel phantom for three-dimensional *in vitro* cell experiments. *Phys Med Biol.* 2009; 54(5):N75-N82.

Altman MB, Stinauer, MA, Javier, D, Aydogan B, Pelizzari, C, Chmura SJ, Roese, JC. Validation of Temporal Optimization for a Single Fraction of Radiation in Vitro. *Int J Rad Onc Biol Phys* (Submitted).

Abstracts Presented at National or International Scientific Conferences:

Altman MB, Vesper BJ, Smith BD, Stinauer, MA, Pelizzari CA, Aydogan B, Radosevich JA, Chmura SJ, Roeske JC. Dosimetric Characterization and Biological Validation of a Novel Phantom for Three-Dimensional IMRT-Based in Vitro Experiments. Med Phys. 35(6): 2816. 2008

Hoggarth MA, Stinauer MA, Altman MB, Roeske JC. Automated Colony Counting Using Color and Image Processing Techniques. Med Phys. 35(6): 2816. 2008

CONCLUSION

Through a series of *in vitro* experiments, we have verified several predictions of a previously performed modeling study. We have demonstrated that, for a single fraction of dose, cell survival can be affected simply by manipulation of the temporal pattern of dose applied during that fraction. It was then shown that these differences are greatest in situations with low-α/β and/or high-β tissues, high doses/fx and long treatment times. Although the effects of temporal dose manipulation need to be further analyzed *in vivo*, the results of both the present work and the modeling study provide a template of how temporal optimization techniques could potentially be used to positively aid treatment outcome, either through increasing cell kill to tumor tissue or enhancing normal tissue sparing.

To test temporal optimization effects in a realistic treatment environment we have created a simple, flexible, and efficient phantom for use in three-dimensional IMRT-based *in vitro* experiments. The simultaneous use of multiple tissue-culture plates provides a three-dimensional grid of biological sample points. By projecting and delivering three-dimensional dose distributions into the cylindrical phantom, radiobiological experiments can be performed in a realistic IMRT setting. Multiple points within the dose delivery volume can be analyzed in a single irradiation session. The TLD and film analysis performed in this study show that IMRT-based dose distributions can be accurately and reliably projected into the phantom under a wide range of experimental designs. Equivalent biological outcome over a range of doses for cells irradiated within the phantom versus those irradiated in a more standard radiobiological setup show that the phantom is a logical progression in the experimental investigation of radiobiological effects in emerging radiation dose delivery technologies.

With the movement towards patient-specified treatment for prostate cancer, including biological parameters and influences, the results of the *in vitro* study showed that temporal optimization techniques could prove to be an important element in enhancing the efficacy of radiation therapy for prostate cancer. The dosimetric accuracy and experimental effectiveness of the phantom make it a good potential tool for analyzing temporal optimization effects *in vitro* using realistic clinical prostate cancer-based treatments.

REFERENCES

[1] Zelefsky MJ, Leibel SA, Gaudin PB*, et al.* Dose escalation with three-dimensional conformal radiation therapy affects the outcome in prostate cancer. *Int J Radiat Oncol Biol Phys* 1998;41:491-500.

[2] Hanks GE, Hanlon AL, Pinover WH*, et al.* Survival advantage for prostate cancer patients treated with high-dose three-dimensional conformal radiotherapy. *Cancer J Sci Am* 1999;5:152-158.

[3] Webb S. Historical perspective on IMRT. In: Palta JR, Mackie TR, editors. AAPM intensity-modulated radiation therapy: the state of the art. Madison, WI: Medical Physics Publishing; 2003. pp. 1-24.

[4] Verhey LJ. Comparison of three-dimensional conformal radiation therapy and intensity-modulated radiation therapy systems. *Semin Radiat Oncol* 1999;9:78-98.

[5] Ezzel G. Clinical implementation of IMRT treatment planning. In: Palta JR, Mackie, TR, editor. Intensity-Modulated Radiation Therapy: The State of the Art. Colorado Springs, CO: Medical Physics Publishing; 2003. pp. 475-494.

[6] Burman C, Chui CS, Kutcher G*, et al.* Planning, delivery, and quality assurance of intensity-modulated radiotherapy using dynamic multileaf collimator: a strategy for large-scale implementation for the treatment of carcinoma of the prostate. *Int J Radiat Oncol Biol Phys* 1997;39:863-873.

[7] Zelefsky MJ, Fuks Z, Happersett L*, et al.* Clinical experience with intensity modulated radiation therapy (IMRT) in prostate cancer. *Radiother Oncol* 2000;55:241-249.

[8] Clark CH, Mubata CD, Meehan CA*, et al.* IMRT clinical implementation: prostate and pelvic node irradiation using Helios and a 120-leaf multileaf collimator. *J Appl Clin Med Phys* 2002;3:273-284.
[9] Nutting CM, Corbishley CM, Sanchez-Nieto B*, et al.* Potential improvements in the therapeutic ratio of prostate cancer irradiation: dose escalation of pathologically identified tumour nodules using intensity modulated radiotherapy. *Br J Radiol* 2002;75:151-161.
[10] Price RA, Hanks GE, McNeeley SW*, et al.* Advantages of using noncoplanar vs. axial beam arrangements when treating prostate cancer with intensity-modulated radiation therapy and the step-and-shoot delivery method. *Int J Radiat Oncol Biol Phys* 2002;53:236-243.
[11] Fowler JF, Welsh JS, Howard SP. Loss of biological effect in prolonged fraction delivery. *Int J Radiat Oncol Biol Phys* 2004;59:242-249.
[12] Benedict SH, Lin PS, Zwicker RD*, et al.* The biological effectiveness of intermittent irradiation as a function of overall treatment time: development of correction factors for linac-based stereotactic radiotherapy. *Int J Radiat Oncol Biol Phys* 1997;37:765-769.
[13] Wang JZ, Li XA. Impact of tumor repopulation on radiotherapy planning. *Int J Radiat Oncol Biol Phys* 2005;61:220-227.
[14] Welsh JS, Howard SP, Fowler JF. Dose rate in external beam radiotherapy for prostate cancer: an overlooked confounding variable? *Urology* 2003;62:204-206.
[15] Bortfeld T, Paganetti H. The biologic relevance of daily dose variations in adaptive treatment planning. *Int J Radiat Oncol Biol Phys* 2006;65:899-906.
[16] Moiseenko V, Duzenli C, Durand RE. In vitro study of cell survival following dynamic MLC intensity-modulated radiation therapy dose delivery. *Med Phys* 2007;34:1514-1520.
[17] Bewes JM, Suchowerska N, Jackson M*, et al.* The radiobiological effect of intra-fraction dose-rate modulation in intensity modulated radiation therapy (IMRT). *Phys Med Biol* 2008;53:3567-3578.
[18] Wang JZ, Li XA, D'Souza WD*, et al.* Impact of prolonged fraction delivery times on tumor control: a note of caution for intensity-modulated radiation therapy (IMRT). *Int J Radiat Oncol Biol Phys* 2003;57:543-552.
[19] Murphy MJ, Lin PS, Ozhasoglu C. Intra-fraction dose delivery timing during stereotactic radiotherapy can influence the radiobiological effect. *Med Phys* 2007;34:481-484.
[20] Zheng XK, Chen LH, Yan X*, et al.* Impact of prolonged fraction dose-delivery time modeling intensity-modulated radiation therapy on hepatocellular carcinoma cell killing. *World J Gastroenterol* 2005;11:1452-1456.
[21] Paganetti H. Changes in tumor cell response due to prolonged dose delivery times in fractionated radiation therapy. *Int J Radiat Oncol Biol Phys* 2005;63:892-900.
[22] Sterzing F, Munter MW, Schafer M*, et al.* Radiobiological investigation of dose-rate effects in intensity-modulated radiation therapy. *Strahlenther Onkol* 2005;181:42-48.
[23] Keall PJ, Chang M, Benedict S*, et al.* Investigating the temporal effects of respiratory-gated and intensity-modulated radiotherapy treatment delivery on in vitro survival: an experimental and theoretical study. *Int J Radiat Oncol Biol Phys* 2008;71:1547-1552.
[24] Kuperman VY, Ventura AM, Sommerfeldt M. Effect of radiation protraction in intensity-modulated radiation therapy with direct aperture optimization: a phantom study. *Phys Med Biol* 2008;53:3279-3292.

[25] Bonner WM. Phenomena leading to cell survival values which deviate from linear-quadratic models. *Mutat Res* 2004;568:33-39.
[26] Carlson DJ, Stewart RD, Li XA*, et al.* Comparison of in vitro and in vivo alpha/beta ratios for prostate cancer. *Phys Med Biol* 2004;49:4477-4491.
[27] Chmura SJ, Farrey K, Wang S*, et al.* Impact of prolonged treatment times. In: Roeske JC, Mundt A, editors. Intensity modulated radiation therapy: a clinical perspecitve: B.C. Decker; 2005. p. 648.
[28] Fowler JF. The radiobiology of prostate cancer including new aspects of fractionated radiotherapy. *Acta Oncol* 2005;44:265-276.
[29] Brenner DJ, Hall EJ. Conditions for the equivalence of continuous to pulsed low dose rate brachytherapy. *Int J Radiat Oncol Biol Phys* 1991;20:181-190.
[30] Brenner DJ. Radiation biology in brachytherapy. *J Surg Oncol* 1997;65:66-70.
[31] Brenner DJ, Hlatky LR, Hahnfeldt PJ*, et al.* The linear-quadratic model and most other common radiobiological models result in similar predictions of time-dose relationships. *Radiat Res* 1998;150:83-91.
[32] Raaphorst GP, Ng CE, Smith D*, et al.* Evidence for adaptive response and implication in pulse-simulated low-dose-rate radiotherapy. *Int J Radiat Oncol Biol Phys* 2000;48:1139-1144.
[33] Yang Y, Xing L. Optimization of radiotherapy dose-time fractionation with consideration of tumor specific biology. *Med Phys* 2005;32:3666-3677.
[34] Altman MB, Chmura SJ, Deasy JO*, et al.* Optimization of the temporal pattern of radiation: an IMRT based study. *Int J Radiat Oncol Biol Phys* 2006;66:898-905.
[35] Lowry R. VassarStats: Statistical Computation Web Site; 2001.
[36] Giard DJ, Aaronson SA, Todaro GJ*, et al.* In vitro cultivation of human tumors: establishment of cell lines derived from a series of solid tumors. *J Natl Cancer Inst* 1973;51:1417-1423.
[37] Lieber M, Smith B, Szakal A*, et al.* A continuous tumor-cell line from a human lung carcinoma with properties of type II alveolar epithelial cells. *Int J Cancer* 1976;17:62-70.
[38] Huang X, Gollin SM, Raja S*, et al.* High-resolution mapping of the 11q13 amplicon and identification of a gene, TAOS1, that is amplified and overexpressed in oral cancer cells. *Proc Natl Acad Sci U S A* 2002;99:11369-11374.
[39] Natarajan N, Shambaugh GE, 3rd, Elseth KM*, et al.* Adaptation of the diphenylamine (DPA) assay to a 96-well plate tissue culture format and comparison with the MTT assay. *Biotechniques* 1994;17:166-171.

APPENDICIES

- Published original peer-reviewed article: Altman *et al.* "Characterization of a novel phantom for three-dimensional *in vitro* cell experiments." *Phys Med Biol.* 2009; 54(5):N75-N82.

Phys. Med. Biol. **54** (2009) N75–N82 doi:10.1088/0031-9155/54/5/N02

NOTE

Characterization of a novel phantom for three-dimensional *in vitro* cell experiments

Michael B Altman[1], Benjamin J Vesper[2,3], Brett D Smith[4], Michelle A Stinauer[4], Charles A Pelizzari[1], Bulent Aydogan[1,4], Chester S Reft[1], James A Radosevich[2,3], Steven J Chmura[1] and John C Roeske[5]

[1] Department of Radiation and Cellular Oncology, University of Chicago, Chicago, IL, USA
[2] Center for Molecular Biology of Oral Diseases, College of Dentistry, University of Illinois at Chicago, Chicago, IL, USA
[3] Jesse Brown VAMC, Chicago, IL, USA
[4] Department of Radiation Oncology, University of Illinois at Chicago, Chicago, IL, USA
[5] Department of Radiation Oncology, Loyola University Medical Center, Maywood, IL, USA

Received 16 September 2008, in final form 10 December 2008
Published 30 January 2009
Online at stacks.iop.org/PMB/54/N75

Abstract
A novel intensity-modulated radiation therapy (IMRT) phantom for use in three-dimensional *in vitro* cell experiments, based on a commercially available system (CIRS Inc., Norfolk, VA), was designed and fabricated. The water-equivalent plastic phantom can, with a set of water-equivalent plastic inserts, enclose 1–3 multi-well tissue culture plates. Dosimetry within the phantom was assessed using thermoluminescence dosimeters (TLDs) and film. The phantom was loaded with three tissue culture plates, and an array of TLDs or a set of three films was placed underneath each plate within the phantom, and then irradiated using an IMRT plan created for it. Measured doses from each dosimeter were compared to those acquired from the treatment planning system. The percent differences between TLD measurements and the corresponding points in the treatment plan ranged from 1.3% to 2.9%, differences which did not show statistical significance. Average point-by-point percent dose differences for each film plane ranged from 1.6% to 3.1%. The percentage dose difference for which 95% of the points in the film matched those corresponding to the calculated dose plane to within 3.0% ranged from 2.8% to 4.2%. The good agreement between predicted and measured dose shows that the phantom is a useful and efficient tool for three-dimensional *in vitro* cell experiments.

1. Introduction

Intensity modulated radiation therapy (IMRT) is a widely used form of external beam radiation therapy (EBRT) in which the beams are modulated during the course of therapy. The

modulation provides the capability to produce radiation fields of non-uniform intensity. IMRT allows the delivered dose distributions to conform more closely to the volume of the target than could generally be achieved through conventional EBRT. The volumetric conformity attainable with IMRT results in a highly variable dose distribution, both spatially and temporally. An increasing number of studies have investigated the effects of applying dose using a variable spatial and/or temporal dose pattern on the underlying biology *in vitro* (Mu *et al* 2003, Suchowerska *et al* 2005, Bromley *et al* 2006, Mackonis *et al* 2007, Sterzing *et al* 2005, Moiseenko *et al* 2007).

However, testing the effects of an IMRT-style dose distribution in a biological setting is not straightforward. Many experiments use a setup where a single cell-containing vessel is encased in a block of water-equivalent material and irradiated using a single fixed beam (Mu *et al* 2003, Suchowerska *et al* 2005, Bromley *et al* 2006, Mackonis *et al* 2007). The dose distributions in these setups are essentially two dimensional, in that the population of cells is irradiated with a single dose pattern. However, in an IMRT-based experiment, there is a need to analyze cell response at discrete positions within the entire three-dimensional treatment volume. In one study, Sterzing *et al* (2005) created a specialized cylindrical phantom to try and resolve these issues. It used an array of nine co-planar sample points acquired using cryotubes; the position of the sample plane was translatable both in the axial and lateral dimensions allowing for sampling of a full three-dimensional space. However, the radiation plan would need to be applied at every position of the array necessary to sample the dose space, limiting its experimental efficiency. Furthermore, irradiation in cryotubes requires plating cells into tissue culture plates or flasks before data acquisition. This introduces more potential experimental error into the results, due in part to the subjugation of the cells to an additional environmental change.

An optimal tool would (1) provide the capability to perform *in vitro* cell experiments three-dimensionally in an IMRT setting, (2) allow for efficient data collection in all three dimensions of the treatment volume, and (3) minimize experimental error by limiting the number of necessary cell transfers. We have created a technique using a simple custom-designed phantom which meets all three of the above challenges.

2. Methods and materials

2.1. IMRT phantom

A cylindrical phantom was designed which is 30 cm long with a 16 cm diameter, based on a commercially available neck phantom (Model 002HN, CIRS Inc., Norfolk, VA). The phantom is composed of a proprietary water-equivalent plastic (CIRS Inc., Norfolk, VA) and contains a custom-cut 86×66 mm^2 rectangular bore extending half the phantom's length. A set of 128×86 mm^2 rectangular inserts, ranging from 1 to 20 mm thick, and an $86 \times 66 \times 35$ mm^3 cap, all made from the same water-equivalent plastic as the rest of the phantom, allow up to three stacked standard multi-well tissue culture plates to be sealed inside the phantom with minimal air gaps (figure 1(a)). The number of wells within a plate can vary, as can plate thickness between manufacturers, although a rectangular 128×86 mm^2 base is standard. As a result, the inserts provide the phantom with a flexibility to manage a wide range of experimental setups (figure 1(b)). To ensure spatial precision, a series of six external guide markers at two axial positions on the phantom are aligned to the in-room laser system. Movement during scanning and treatment is prevented by placing the phantom on a plastic stand molded to the curvature of the phantom. Both the stand and the guide markers are components of the original CIRS Model 002HN phantom.

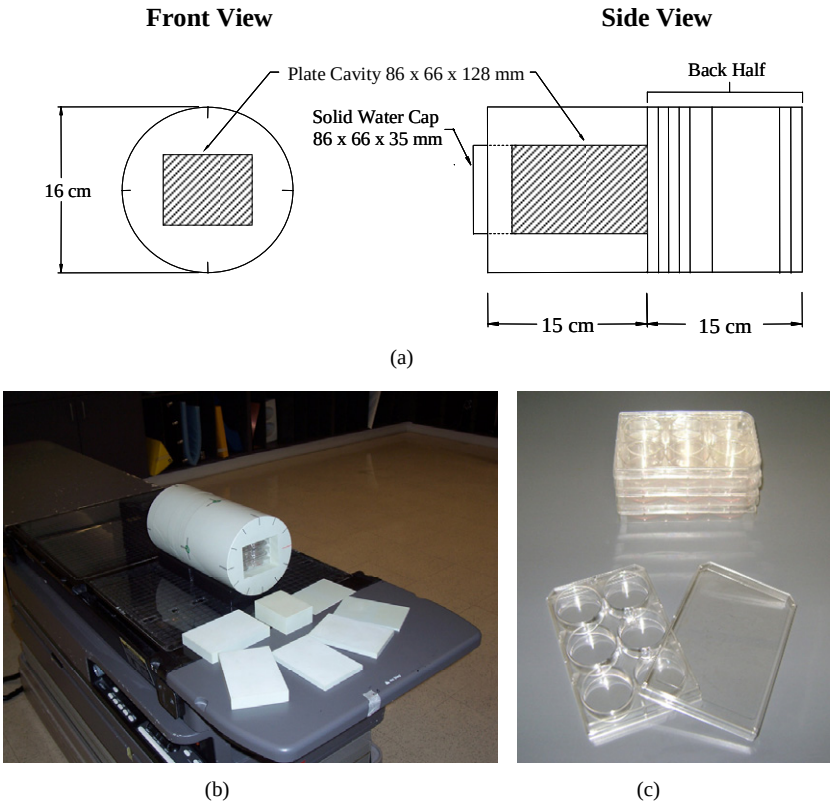

Figure 1. (a) Phantom schematic. Multi-well cell culture plates can be placed into the cavity during experiments. The zone labeled 'back half' contains markers and chambers for use with an array of dosimeters and is the same as that in the Model 002HN CIRS phantom. (b) Phantom loaded with tissue culture plates and inserts. (c) Single six-well tissue culture plate and lid (front). Stack of three six-well plates (back).

(This figure is in colour only in the electronic version)

2.2. Dosimetric characterization

The phantom is designed to work with standard multi-well tissue culture plates, which are generally single pieces of molded polystyrene plastic with separate fitted lids (figure 1(c)). The wells are a rectangular array of, essentially, 'mini Petri dishes' recessed from the top of the plate. Under experimental conditions, the stacked well plates present a matrix of plastic, liquid (filling the wells), and air pockets. Hence, the factor which could potentially have the greatest adverse affect on accurate dose delivery within the phantom under experimental conditions is these air gaps within the plates between the cells and the phantom walls. To assess the maximum impact of these air gaps, phantom dosimetry was characterized with both thermoluminescence dosimeters (TLDs) and film using a 'worst case' experimental setup in terms of air in the plate containing chamber. A clonogenic survival assay setup, resulting in air occupying ∼75% of the plate chamber volume, was used: a stack of three 2.2 cm thick six-well tissue culture plates (Corning Inc., Corning, NY) filled with 2 mL H_2O per well. A CT (PQ5000, Philips Medical Systems, Andover, MA) scan of the plate-filled phantom was obtained. An IMRT plan for this CT scan was generated using the Eclipse treatment planning

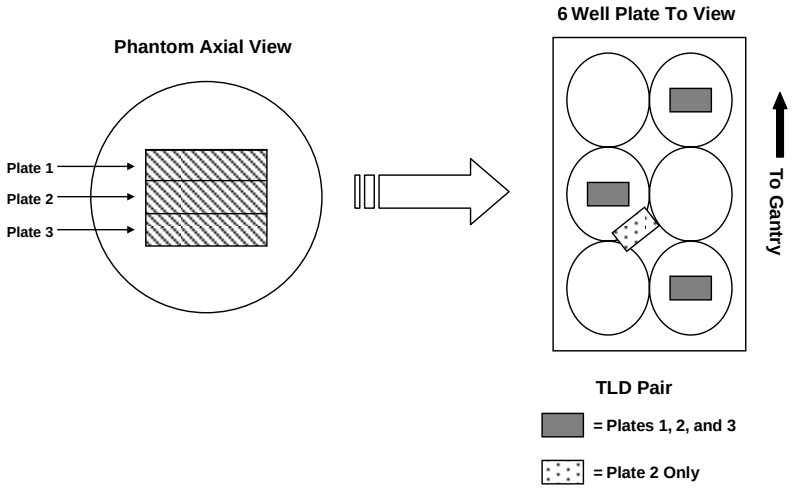

Figure 2. Schematic six-well plate placement within the phantom (left) and placement of ten TLD pairs on the bottom of plates 1, 2 and 3 within the phantom (right). Dark grey rectangles denote TLD locations common to all three plates. Dotted rectangles denote TLD locations on plate 2 only.

system (Varian Corporation, Palo Alto, CA) containing a single planning target volume (PTV) encompassing all three plates with mean dose 200.9 cGy and $\sigma^2 = 4.53$ cGy. Six equally spaced beam angles were used, ranging from 28° to 336°. Dose calculations were performed using the analytical anisotropic algorithm (AAA) (Ulmer and Kaissl 2003, Ulmer *et al* 2005). All irradiations in this study were performed using a clinical linear accelerator (2100CD, Varian Medical Systems, Palo Alto, CA).

A set of TLDs with dimensions $0.038 \times 0.32 \times 0.32$ cm^3 and sensitivities with standard deviations $<1\%$ was determined using the methods described by Al Hallaq *et al* (2006) with a Harshaw 3500 TLD Reader (Thermo Fisher Scientific Inc., Waltham, MA). Individual TLD sensitivity correction factors were determined from this process and used to correct all the subsequent TLD measurements. Pairs of TLDs were placed at ten locations among the three water-filled plates, which were then loaded in the phantom (figure 2). The TLDs were placed on the underside of the water-filled wells in the plate as cells adhere to the floor of the wells in the clonogenic assay. Such a placement puts the TLDs (as with the film, discussed below) as close to the position of the cells under experimental conditions as possible while keeping them dry.

The phantom was irradiated with the clinical linear accelerator using the IMRT plan. This was repeated twice, each time placing the same TLD at the same position in the phantom. Each IMRT delivery included calibrated TLDs to convert the TLD readings to absorbed dose. The predicted doses to the TLDs were calculated in Eclipse. Systematic errors in the TLD measurements were determined to be 1.5% from the initial calibration. Individual TLD random errors were assumed to be the standard deviations of the three independent in-phantom measured doses. The systematic error in the treatment planning calculated doses was estimated at 3.0% (Khan 2003, Aydogan *et al* 2007, Sanchez-Doblado *et al* 2007). The random errors in calculated dose were determined from standard deviations of dose in the volumes used to determine the expected TLD doses. The total errors were determined by adding the corresponding random and systematic errors in quadrature. The Student's *t*-test was then used to analyze the difference between measured and calculated TLD doses.

Table 1. Comparison between measured and calculated TLDs dose.

	Measured dose (cGy)		Calculated dose (cGy)		
TLD number	Average	σ	Average	σ	Percent difference[a]
1	206.2	1.1	208.2	0.3	1.0%
2	205.4	1.0	208.1	0.3	1.3%
3	200.3	1.8	203.8	0.3	1.7%
4	199.2	2.0	203.7	0.2	2.2%
5	197.8	1.0	203.6	0.2	2.9%
6	200.6	1.3	203.8	0.2	1.6%
7	204.1	0.6	205.8	0.3	0.8%
8	205.7	1.0	205.8	0.3	0.0%
9	200.2	1.5	202.7	0.2	1.2%
10	203.0	0.8	202.7	0.1	−0.2%
11	200.1	0.2	203.1	0.4	1.5%
12	199.5	3.0	202.7	0.4	1.6%
13	197.3	1.4	201.3	0.2	2.0%
14	198.3	1.7	201.4	0.1	1.5%
15	203.2	3.0	201.6	0.4	−0.8%
16	204.9	1.0	202.2	0.4	−1.3%
17	199.4	4.0	199.7	0.4	0.2%
18	200.2	4.4	200	0.5	−0.1%
19	199.3	5.0	197.4	0.4	−1.0%
20	197.8	1.6	197.9	0.4	0.0%

Abbreviations: TLD = thermoluminescent dosimeter, σ = standard deviation.
[a] Percent difference is between average measured and calculated dose. All values show no statistically significant differences ($p > 0.05$).

The treatment plan was then delivered with Kodak EDR2 film (Eastman Kodak Company, Rochester, NY) cut to plate dimensions and placed below each well plate, yielding three films. Each film was irradiated individually within the phantom, as a 1–3% error was found due to the large volume of air in the phantom setup when the films were irradiated together (data not shown). Following irradiation, films were processed using a Kodak X-Omat 3000RA (Eastman Kodak Company, Rochester, NY) and digitized with an Epson Expression 10000XL flat-bed scanner (Epson America Inc., Long Beach, CA). The phantom-irradiated films were then registered to corresponding dose plane images extracted from Eclipse using pre-existing software developed at the University of Illinois at Chicago. Due to the lack of steep dose gradients within the treatment plan, the absolute percentage dose difference ($\%D_{\text{diff}}$) between corresponding pixels in the film and predicted dose plane images was used to compare the films in this study. The mean $\%D_{\text{diff}}$ was calculated for all pixels within the interior 90% of each film image, eliminating errors due to edge effects. For each film, the $\%D_{\text{diff}}$ at which 95% of the points in the image were equal to or below that cutoff ($\%D_{\text{diff,95}}$) was also calculated.

3. Results

The average TLD dose from three independent measurements in the phantom ranged from 197.3 to 206.2 cGy, while the doses at those points predicted by the treatment planning software ranged from 197.4 to 208.1 cGy (table 1). The signed percent differences in table 1 indicate whether the measured TLD dose was lower (negative) or higher (positive) than the predicted dose and range from −1.33% to 2.86%. For all TLDs, *t*-test comparison of measured and predicted doses revealed $p > 0.05$. This implies that the aforementioned percent differences

Table 2. Measured doses for the three films displayed in figure 2 and calculated doses of the corresponding dose planes from the treatment planning system.

	Dose (cGy)						
	Measured		Calculated		$\%D_{\text{diff}}$ (%)		
	Mean	σ	Mean	σ	Mean	σ	$\%D_{\text{diff,95}}$ (%)
Film 1	197.7	2.3	202.3	3.9	2.6	0.8	3.8
Film 2	195.7	2.3	201.5	4.3	3.1	0.6	4.2
Film 3	195.6	2.5	198.9	3.7	1.6	0.7	2.8

Abbreviations: σ = standard deviation, $\%D_{\text{diff}}$ = percentage dose difference, $\%D_{\text{diff,95}}$ = the percentage dose difference at which 95% of all points in the images agree.

do not show statistical significance. Hence the doses projected into the phantom match those actually delivered at the TLD locations even in the highly inhomogeneous environment of the well-plate-filled phantom.

Table 2 displays the average dose and standard deviation of dose for each measured film, those same factors for the corresponding treatment plan calculated dose planes, as well as $\%D_{\text{diff}}$ comparisons for those planes. Note the good general agreement for all three films ($\%D_{\text{diff}}$ ranged from 1.6% to 3.1%, while $\%D_{\text{diff,95}}$, ranged from 2.8% to 4.2%). It could be argued that Film 3, located at the tissue culture plate/water-equivalent plastic (plate/plastic) interface showed the better agreement than the other two films, in that it had the lowest measured $\%D_{\text{diff}}$ and $\%D_{\text{diff,95}}$ values. However, EDR2 film can be an inconsistent dosimeter in and around inhomogeneities and/or air gaps (Charland *et al* 2003, Chetty and Charland 2002, Yoon *et al* 2007, Gillis *et al* 2005, Pai *et al* 2007). The use of prolonged irradiation with multiple IMRT-type fields could also result in film under response due to the Schwarzschild effect (Djouguela *et al* 2005). Thus, although the differences increase slightly away from the plate/plastic interface, this could largely be explained by the inaccuracies of film as a dosimeter in those environments. There is also a 3.0% error in the treatment planning calculated dose, as noted in section 2.2. Given these and the overall small magnitudes of $\%D_{\text{diff}}$ and $\%D_{\text{diff,95}}$, the measured film doses agree well with those projected into the phantom.

4. Discussion

We have created a novel phantom to easily and efficiently perform *in vitro* cell experiments in a fully three-dimensional IMRT setting. Up to three stacked multi-well tissue culture plates can be placed inside the cylindrical, water-equivalent plastic phantom along with a series of inserts to minimize unnecessary air gaps, a setup providing a three-dimensional array of *in vitro* experiments. A strength of this design is its simplicity; as the phantom could be easily replicated in a machine shop, many research centers could perform experiments using it. Although simple, the phantom proves advantageous in terms of experimental technique. As the plate space is large compared to other previous experimental designs, the phantom provides a far more complete and/or efficient biological sampling of a three-dimensional IMRT dose space than any of the previously used techniques. Furthermore, the phantom has no moving parts, and requires no specialized equipment or water filling to use, enhancing its efficiency compared to other methods.

Measured dosimetry within the phantom analyzed under experimental conditions using both TLDs and film agreed well with the dose projected into the phantom by the treatment planning system. The phantom is designed for potential use in irradiation schemes with large

dose homogeneities. We did not irradiate with such a plan, as the clonogenic setup we have used requires large sample spaces (i.e. the whole well would be irradiated with a constant dose). Furthermore, the configurations with sufficient biological sample frequency for more complex dose distributions would use either plates with higher number wells/plate or 'single well' plates (essentially a Petri dish with multi-well plate base dimensions). These plates are generally thinner than those which we used and, when filled, would result in far less air by volume in the plate than the experimental setup we employed. This, in combination with the accuracy in the worst case experimental setup, implies the phantom could be reliably used in any configuration and with any dose distribution.

As well plates with any number of wells will fit inside the phantom, assays which require cells to adhere to the well floor or free float in media are both possible, provided a well of sufficient size is chosen to allow for the desired dose space sampling. All of these factors mean any assay performed using well plates is feasible, including those at the cutting edge of radiation therapy research. Gene microarry analysis of genes coding for radiosensitivity (Torres-Roca *et al* 2005, Wong *et al* 2006), radiation-based studies of $\gamma-$H2AX, a marker for DNA double strand breaks, (Kao *et al* 2006) and several enzyme-linked immunosorbent assay (ELISA) studies (Kaminski *et al* 2005, Zhao *et al* 2008, Fleckenstein *et al* 2007) have all addressed a number of radiation-therapy-related issues. The phantom provides a simple, efficient platform to put future similar experiments into a realistic, treatment-based environment: patient-based three-dimensional dose distributions could be delivered, allowing for multiple biological samples from a wide array of points within the treatment volume.

The simplicity and flexibility of the phantom design allow it to be used with a wide range of current and emerging radiation delivery systems. The phantom is easily adapted to use in experiments with any clinical linac, tomotherapy system, or even stereotactic radiotherapy devices. Ultimately, as the diversity and complexity in the technology of radiation therapy and radiobiological research increases, the biological and technological flexibility of the phantom, along with its extreme efficiency as an experimental tool, makes it an immensely useful and potentially important tool in the understanding of the underlying radiobiology of modern radiation therapy.

5. Conclusion

We have created a simple, flexible and efficient phantom for use in three-dimensional IMRT-based *in vitro* experiments. The simultaneous use of multiple tissue-culture plates provides a three-dimensional grid of biological sample points, allowing for biological experiments to be performed in a realistic IMRT setting. This provides a number of improvements in experimental technique over other previously used apparatuses, including the ability to sample a large number of points within the dose delivery volume in a single irradiation session and the use of cell culture plates to minimize the experimental error. The TLD and film analysis show that IMRT-based dose distributions can be accurately and reliably projected into the phantom under a wide range of experimental setups. These factors make the phantom a potentially important tool in the understanding of radiobiology principles that have a direct impact on the efficacy of radiation therapy.

Acknowledgments

This work was partially supported by a grant from MedImmune and partially supported by the Department of Defense Prostate Cancer Research Program under award number W81XWH-

08-1-0189. Views and opinions of and endorsements by the authors do not reflect those of the US Army or the Department of Defense.

References

Al-Hallaq H A, Reft C S and Roeske J C 2006 The dosimetric effects of tissue heterogeneities in intensity-modulated radiation therapy (IMRT) of the head and neck *Phys. Med. Biol.* **51** 1145–56

Aydogan B, Tiryaki H, Al-Hallaq H A and Roeske J C 2007 Verification of lung tumor doses calculated by the eclipse AAA and pinnacle CC algorithms (abstract) *Med. Phys.* **34** 2521

Bromley R, Davey R, Oliver L, Harvie R and Baldock C 2006 A preliminary investigation of cell growth after irradiation using a modulated x-ray intensity pattern *Phys. Med. Biol.* **51** 3639–51

Charland P M, Chetty I J, Yokoyama S and Fraass B A 2003 Dosimetric comparison of extended dose range film with ionization measurements in water and lung equivalent heterogeneous media exposed to megavoltage photons *J. Appl. Clin. Med. Phys.* **4** 25–39

Chetty I J and Charland P M 2002 Investigation of Kodak extended dose range (EDR) film for megavoltage photon beam dosimetry *Phys. Med. Biol.* **47** 3629–41

Djouguela A, Kollhoff R, Rubach A, Harder D and Poppe B 2005 The Schwarzschild effect of the dosimetry film Kodak EDR 2 *Phys. Med. Biol.* **50** N317–21

Fleckenstein K, Gauter-Fleckenstein B, Jackson I L, Rabbani Z, Anscher M and Vujaskovic Z 2007 Using biological markers to predict risk of radiation injury *Semin. Radiat. Oncol.* **17** 89–98

Gillis S, De Wagter C, Bohsung J, Perrin B, Williams P and Mijnheer B J 2005 An inter-centre quality assurance network for IMRT verification: results of the ESTRO QUASIMODO project *Radiother. Oncol.* **76** 340–53

Kaminski M S *et al* 2005 131I-tositumomab therapy as initial treatment for follicular lymphoma *N. Engl. J. Med.* **352** 441–9

Kao J, Milano M T, Javaheri A, Garofalo M C, Chmura S J, Weichselbaum R R and Kron S J 2006 gamma-H2AX as a therapeutic target for improving the efficacy of radiation therapy *Curr. Cancer Drug Targets* **6** 197–205

Khan F M 2003 *The Physics of Radiation Therapy* (Philadelphia, PA: Lippincott Williams & Wilkins)

Mackonis E C, Suchowerska N, Zhang M, Ebert M, Mckenzie D R and Jackson M 2007 Cellular response to modulated radiation fields *Phys. Med. Biol.* **52** 5469–82

Moiseenko V, Duzenli C and Durand R E 2007 *In vitro* study of cell survival following dynamic MLC intensity-modulated radiation therapy dose delivery *Med. Phys.* **34** 1514–20

Mu X, Lofroth P O, Karlsson M and Zackrisson B 2003 The effect of fraction time in intensity modulated radiotherapy: theoretical and experimental evaluation of an optimisation problem *Radiother. Oncol.* **68** 181–7

Pai S, Das I J, Dempsey J F, Lam K L, Losasso T J, Olch A J, Palta J R, Reinstein L E, Ritt D and Wilcox E E 2007 TG-69: radiographic film for megavoltage beam dosimetry *Med. Phys.* **34** 2228–58

Sanchez-Doblado F, Hartmann G H, Pena J, Capote R, Paiusco M, Rhein B, Leal A and Lagares J I 2007 Uncertainty estimation in intensity-modulated radiotherapy absolute dosimetry verification *Int. J. Radiat. Oncol. Biol. Phys.* **68** 301–10

Sterzing F, Munter M W, Schafer M, Haering P, Rhein B, Thilmann C and Debus J 2005 Radiobiological investigation of dose-rate effects in intensity-modulated radiation therapy *Strahlenther. Onkol.* **181** 42–8

Suchowerska N, Ebert M A, Zhang M and Jackson M 2005 *In vitro* response of tumour cells to non-uniform irradiation *Phys. Med. Biol.* **50** 3041–51

Torres-Roca J F *et al* 2005 Prediction of radiation sensitivity using a gene expression classifier *Cancer Res.* **65** 7169–76

Ulmer W and Kaissl W 2003 The inverse problem of a Gaussian convolution and its application to the finite size of the measurement chambers/detectors in photon and proton dosimetry *Phys. Med. Biol.* **48** 707–27

Ulmer W, Pyyry J and Kaissl W 2005 A 3D photon superposition/convolution algorithm and its foundation on results of Monte Carlo calculations *Phys. Med. Biol.* **50** 1767–90

Wong Y F, Sahota D S, Cheung T H, Lo K W, Yim S F, Chung T K, Chang A M and Smith D I 2006 Gene expression pattern associated with radiotherapy sensitivity in cervical cancer *Cancer J.* **12** 189–93

Yoon M, Lee D H, Shin D, Lee S B, Park S Y and Cho K H 2007 Accuracy of inhomogeneity correction algorithm in intensity-modulated radiotherapy of head-and-neck tumors *Med. Dosim.* **32** 44–51

Zhao L *et al* 2008 The predictive role of plasma TGF-beta1 during radiation therapy for radiation-induced lung toxicity deserves further study in patients with non-small cell lung cancer *Lung Cancer* **59** 232–9